

**$\pi$ - $K$  scattering lengths at finite temperature in the  
Nambu–Jona-Lasinio model**

P. Piwnicki, S. P. Klevansky and P. Rehberg

*Institut für Theoretische Physik,*

*Philosophenweg 19, D-69120 Heidelberg, Germany*

Abstract

The transition amplitude for  $\pi K$  scattering is evaluated within the SU(3) Nambu–Jona-Lasinio model. Ordering terms according to the expansion in  $1/N_c$  leads to a box-like diagram,  $t$  channel diagrams that admit scalar isoscalar ( $\sigma, \sigma'$ ) exchanges, and a  $u$  channel exchange of a scalar isodoublet  $\sigma_K$  that has quantum numbers corresponding to the  $K_0^*(1430)$ . Both the Pauli-Villars and O(3) regularization procedures are used to evaluate the  $T = 0$  values of the  $l = 0$  scattering lengths  $a_0^{3/2}$  and  $a_0^{1/2}$ . The finite temperature dependence is studied. We find that the variation in the  $t$  channel in the calculation of  $a_0^{3/2}$  leads to a change in  $a_0^{3/2}$  of a factor of about two over the temperature range of  $T = 150$  MeV.

PACS: 11.30.Rd; 13.75.Lb; 14.40.Aq; 11.10.Wx.

Keywords: finite temperature scattering lengths; Nambu–Jona-Lasinio model;

## I. INTRODUCTION

The pseudoscalar octet ( $\pi, K, \eta$ ) forms the set of lowest mass hadronic states and are thus particles that play a central role in heavy ion collisions, since they occur copiously. In particular the pion, with lowest mass and being an isospin triplet has a central role, while the kaonic sector, occurring as isospin doublets, gives us information on strangeness production. Since this octet consists of the Goldstone bosons associated with spontaneous chiral symmetry breaking, their role in nature is determined almost exclusively by this feature. Conversely, our understanding of chiral symmetry breaking is augmented by studying the properties of such mesons, and this can be extended to finite temperatures and baryon density.

The purpose of this paper is to examine elastic  $\pi K \rightarrow \pi K$  scattering in particular at  $T = 0$  and at finite temperatures. Expressions for the transition amplitudes and hence the scattering lengths at  $T = 0$  are derived and then the temperature dependence of the scattering lengths is investigated. This is of interest (a) in its own right, although at present it is unclear how one would access finite temperature scattering lengths experimentally, and (b) as it provides a first step in the calculation of the elastic  $\pi K \rightarrow \pi K$  cross-sections as a function of the temperature that are required as input for the collision dynamics for a simulation of heavy-ion collisions using a chiral Lagrangian.

At  $T = 0$ ,  $\pi K$  scattering has been studied within the framework of chiral perturbation theory (CHPT) [1–3]. It is not *a priori* clear to what extent a chiral expansion is appropriate for properties involving the strange quark, in view of its mass. Yet the results of even the early calculations of the scattering lengths<sup>1</sup> [1] fall within the expected measured range [5–7], although one should note that actual

---

<sup>1</sup> There is an early Russian publication on this subject that we also draw the reader's

experimental values are rather poorly known. An elaboration of this approach that includes intermediate resonances [2], in particular the exchange of the vector  $K^*$  in the  $u$ -channel as well as of a  $\rho$ -meson in the  $t$ -channel, alters the actual numerical values by 2% at most.

In this paper, we wish to examine the  $\pi K$  scattering lengths at finite temperature. The Nambu–Jona-Lasinio (NJL) model [8,9] gives a good description of these deeply bound mesons at  $T = 0$ . In obtaining such a description, the mean field or Hartree approximation to the self-energy, together with the random phase approximation for the mesonic fields has been used. It has been recognized that these approximations taken together constitute an expansion in the inverse number of colors  $1/N_c$ , within the model [10,11] and are essential in order to preserve the chiral symmetry of the underlying Lagrangian. For  $T \neq 0$ , the dependence of some of the pseudoscalar and scalar mesons as a function of temperature has qualitatively been validated by lattice gauge calculations [12,13]. The results of Ref. [13] display a remarkable qualitative agreement with the finite temperature behavior of the NJL model (pole) masses. This gives one some confidence in the application of this model in this form to finite temperature, although it is speculative.

In addition, it can be shown that the current algebra results or alternatively the results of chiral perturbation theory to lowest order can be obtained from this model on making a suitable chiral expansion [14,15]. It is then a simple issue to extend calculations to finite temperature, and examine the consequences thereof. There is no necessity to enforce the chiral limit, since this is a model study. We thus examine the three flavor NJL model. Contributions to the scattering amplitude are organized according to the expansion in  $1/N_c$ . To lowest order within this scheme,

---

attention to [4]

there are several sorts of graphs that occur: a box graph is present, analogous to the four-point tree-like structure of mesonic theories. In addition, in the  $t$  channel, exchange of neutral scalars, in this case the  $\sigma_0$  and  $\sigma_8 \rightarrow \sigma$  and  $\sigma'$  states occur. This has no counterpart in the CHPT version <sup>2</sup>. Finally, the  $u$  channel contains the exchange of a  $\sigma_K$ , corresponding to the  $K_0^*$  meson – note that this also differs from the CHPT calculations that explicitly include vector resonance exchange of the  $K^*$  [2]. Note that in our case, no six point tadpole-like diagrams [1] are present. In addition, unitarising graphs that include  $\pi K$  scattering in the intermediate state are not included to this lowest order in  $1/N_c$  calculation of the scattering lengths in the NJL model, but which would be essential for a complete description of the scattering amplitude of cross section calculated as a function of center of mass energy.

Before discussing our results, we comment on the procedure that is to be taken, in particular with regard to the application of the mean field plus random phase approximation at  $T = 0$  and at  $T \neq 0$ . As discussed earlier, this coupled symmetry preserving approximation works excellently at  $T = 0$ . This is true for calculating static mesonic properties, such as masses, mean charge radii and scattering lengths, particularly in the SU(2) sector, where these have been studied in detail and are well-known. Corrections to the mean field values introduce chiral logarithms, see for example [16] and further powers in the pion mass. Calculations of the full scattering cross-sections, however, do require these corrections, even at  $T = 0$ , in order to preserve unitarity. Thus only scattering lengths can be reliably calculated. This is

---

<sup>2</sup>Note that no  $\rho$ -meson can be exchanged in this minimal version of the NJL model, but would also be of the same order as the  $\sigma$  exchanges in the  $1/N_c$  expansion within an extended NJL model [15]. For this reason, we do not calculate the  $l = 1$  scattering lengths  $a_1^{1/2}$ ,  $a_1^{3/2}$ .

well-established for the two flavor case [17] and is the reason for our restriction to investigating this quantity only.

In extending our calculation to finite temperature, we are being speculative, encouraged however, by the success of the qualitative agreement of the lattice predictions of the temperature variation of particle masses with those predicted by the model. Furthermore, it is not expected that terms beyond this leading  $1/N_c$  calculation play a dominant role, since the chiral logarithms and powerlike mass terms that might then occur depend then on the temperature dependent pion mass, which in turn stays constant within the model for a wide range of temperatures, even up to 200 MeV. The divergences that have been found in this work in the scattering lengths are induced by the presence of the inverse of the decay constants which themselves become small at high temperatures. This feature should remain unchanged by higher order corrections.

Our model results depend on the regularization procedure used, and can therefore at most be qualitative. While the Pauli-Villars method is generally preferred at  $T = 0$  since it preserves all symmetries, and enables one to check that the crossing symmetries are correctly implemented, at  $T \neq 0$ , Lorentz invariance is broken by the heat bath so that a three dimensional cutoff can be used. We thus only expect to obtain a qualitative description. We evaluate the scattering lengths at  $T = 0$  using both prescriptions, and considering parameters sets of other authors [19,20,9] that were used for different purposes to fix other variables. In this sense, we do not fit model parameters so as to explicitly give us good values of the scattering lengths. Our results at  $T = 0$  are obtained using both regularization schemes. At finite temperatures, we find that the  $t$  channel varies somewhat with temperature due to the exchange of the scalar mesons, which themselves have a strong temperature dependence, and we find that the variation of  $a_0^{3/2}$  in particular, is visible. At

$T = 150$  MeV, the  $T = 0$  value is increased by a factor of 2.36. This is in contrast to the temperature dependence found for the  $\pi\pi$  scattering lengths [21] which show almost no change over  $T = 0$  to 150 MeV. The value of  $a_0^{1/2}$  changes only slightly, increasing in this case only by a factor of 1.18.

This paper is organized as follows. In Section II, we give a brief introduction to the NJL Lagrangian, sufficient to introduce our notation. In Section III, we classify the scattering diagrams required for elastic  $\pi K$  scattering within the framework of the model and examine in particular the reaction  $\pi^+ K^+ \rightarrow \pi^+ K^+$ . This is studied explicitly at  $T = 0$  in Sec. IV A and the scattering lengths for this process as well as the remaining  $\pi K$  processes, which can be obtained via crossing symmetry, are then evaluated. In Sec. IV B, the generalization to finite temperature is discussed. We summarize and conclude in Sec. V.

## II. SU(3) NAMBU–JONA-LASINIO MODEL

The SU(3) NJL model is well documented elsewhere [8,9]. In this section, we give only a brief description of the model in order to introduce our notation. Our starting point is the minimal three flavor chiral Lagrangian density

$$\begin{aligned} \mathcal{L}_{\text{chiral}} = & \bar{\psi} i \not{\partial} \psi + G \sum_{a=0}^8 \left[ (\bar{\psi} \lambda^a \psi)^2 + (\bar{\psi} i \gamma_5 \lambda^a \psi)^2 \right] \\ & - K \left[ \det(\bar{\psi}(1 + \gamma_5)\psi) + \det(\bar{\psi}(1 - \gamma_5)\psi) \right] \end{aligned} \quad (2.1)$$

that contains a four point coupling with strength  $G$ , and six point coupling, with coupling strength  $K$ . Color, flavor and spinor indices of the quark fields  $\psi$  are suppressed. The term moderated by  $G$  contains the Gell-Mann matrices  $\lambda^a$ ,  $a = 1..8$  plus the matrix  $\lambda^0 = \sqrt{2/3}I$ , where  $I$  is the unit matrix, thereby ensuring the U(3) symmetry of this term. This symmetry is broken by the determinantal term,

motivated by instanton effects, down to the chiral group  $SU_L(3) \times SU_R(3)$ . In order to incorporate the known current quark masses, an additional term that explicitly breaks the chiral symmetry,

$$\mathcal{L}_{\text{mass}} = -(m_u^0 \bar{u}u + m_d^0 \bar{d}d + m_s^0 \bar{s}s) \quad (2.2)$$

must be introduced, so that  $\mathcal{L}_{\text{NJL}} = \mathcal{L}_{\text{chiral}} + \mathcal{L}_{\text{mass}}$ .

A straightforward evaluation of the self-energy in the mean field approximation yields constituent quark masses that are modified from their current values due to dynamical symmetry breaking [19,8]

$$m_i = m_i^0 + 4iGN_c \text{tr}S^i - 2KN_c^2 (\text{tr}S^j)(\text{tr}S^k), \quad i \neq j \neq k \neq i \quad , \quad (2.3)$$

where the propagator  $S^i(x, x')$  satisfies

$$(i \not{\partial}_x - m_i)S^i(x, x') = \delta^{(4)}(x - x') \quad (2.4)$$

in the mean field approximation and  $i$  is a flavor index.

The mesonic sector is viewed most simply from the effective NJL Lagrangian that is obtained on constructing an effective four point interaction from the six point term, on contraction of two fermionic fields. One has

$$\begin{aligned} \mathcal{L}_{\text{chiral}} = & \bar{\psi} i \not{\partial} \psi + \sum_{i=0}^8 \left[ K_i^{(-)} (\bar{\psi} \lambda^i \psi)^2 + K_i^{(+)} (\bar{\psi} i \gamma_5 \lambda^i \psi)^2 \right] \\ & + \left[ \frac{1}{2} K_m^{(-)} (\bar{\psi} \lambda^8 \psi) (\bar{\psi} \lambda^0 \psi) + \frac{1}{2} K_m^{(+)} (\bar{\psi} i \gamma_5 \lambda^8 \psi) (\bar{\psi} i \gamma_5 \lambda^0 \psi) \right] \\ & + \left[ \frac{1}{2} K_m^{(-)} (\bar{\psi} \lambda^0 \psi) (\bar{\psi} \lambda^8 \psi) + \frac{1}{2} K_m^{(+)} (\bar{\psi} i \gamma_5 \lambda^0 \psi) (\bar{\psi} i \gamma_5 \lambda^8 \psi) \right] \end{aligned} \quad (2.5)$$

with the effective couplings

$$K_0^{(\pm)} = G \mp \frac{1}{3} N_c K (i \text{tr}S^s + 2i \text{tr}S^u)$$

$$\begin{aligned}
K_1^{(\pm)} &= K_2^{(\pm)} = K_3^{(\pm)} = G \pm \frac{1}{2} N_c K i \text{tr} S^s \\
K_4^{(\pm)} &= K_5^{(\pm)} = K_6^{(\pm)} = K_7^{(\pm)} = G \pm \frac{1}{2} N_c K i \text{tr} S^u \\
K_8^{(\pm)} &= G \mp \frac{1}{6} N_c K (i \text{tr} S^s - 4 i \text{tr} S^u) \\
K_m^{(\pm)} &= \mp \frac{\sqrt{2}}{3} N_c K (i \text{tr} S^s - i \text{tr} S^u) \quad , \quad (2.6)
\end{aligned}$$

in the case  $m_u^0 = m_d^0$ . Both scalar and pseudoscalar octet channels may be identified by the isospin operator correspondence

$$\begin{aligned}
\lambda_3 &\rightarrow \pi^0, \sigma_\pi \\
\frac{1}{\sqrt{2}}(\lambda_1 \pm i\lambda_2) &\rightarrow \pi^{(\pm)}, \sigma_\pi^{(\pm)} \\
\frac{1}{\sqrt{2}}(\lambda_6 \pm i\lambda_7) &\rightarrow K^0, \bar{K}^0, \sigma_K^0, \bar{\sigma}_K^0 \\
\frac{1}{\sqrt{2}}(\lambda_4 \pm i\lambda_5) &\rightarrow K^{(\pm)}, \sigma_K^{(\pm)} \quad , \quad (2.7)
\end{aligned}$$

using an obvious notation for the scalar sector. Experimentally, one could tentatively assign the scalar particles  $(\sigma_\pi, \sigma_K) \rightarrow (a_0(980), K_0^*(1430))$ . The assignment of the  $(\sigma, \sigma')$  to actual particles such as the controversial  $f_0(400-1200)$  or  $\sigma$  [22] or  $f_0(980)$  and  $f_0(1300)$  is uncertain and we thus retain our model notation here. The pionic and kaonic scalar and pseudoscalar sectors can be treated independently now. The quark-antiquark scattering amplitude, evaluated in the random phase approximation is

$$M_{\pi, \sigma_\pi} = \frac{2K_1^{(\pm)}}{1 - 2K_1^{(\pm)} \Pi_{P,S}^{q\bar{q}}(k^2)} \quad (2.8)$$

for the pions, or

$$M_{K, \sigma_K} = \frac{2K_4^{(\pm)}}{1 - 2K_4^{(\pm)} \Pi_{P,S}^{s\bar{q}}(k^2)} \quad , \quad (2.9)$$

for the kaons, expressed in terms of the irreducible polarization

$$-i\Pi_{P,S}^{f_1 f_2}(k^2) = -2N_c \int \frac{d^4 q}{(2\pi)^4} \text{tr}[iS^{f_1}(p+q)\Gamma^{P,S} iS^{f_2}(q)\Gamma^{P,S}] \quad . \quad (2.10)$$



Here  $f_1$  and  $f_2$  refer to the quark flavors  $q = u, d$  and  $s$ . The indices  $P, S$  refer to pseudoscalar or scalar functions respectively, and  $\Gamma^P = i\gamma_5$ , while  $\Gamma^S = 1$ . The meson masses with the appropriate quantum numbers are obtained by solving

$$\begin{aligned} 1 - 2K_1^{(\pm)}\Pi_{P,S}^{q\bar{q}}(k^2) &= 0 \\ 1 - 2K_4^{(\pm)}\Pi_{P,S}^{s\bar{q}}(k^2) &= 0 \end{aligned} \quad (2.11)$$

for the pionic or kaonic masses respectively, while the associated couplings are given as

$$g_{M_\pi qq}^2 = \left( \frac{\partial \Pi_{P,S}^{q\bar{q}}}{\partial k^2} \right)_{k^2=m_{M_\pi}^2}^{-1} \quad g_{M_K sq}^2 = \left( \frac{\partial \Pi_{P,S}^{s\bar{q}}}{\partial k^2} \right)_{k^2=m_{M_K}^2}^{-1} . \quad (2.12)$$

In this equation,  $M_\pi$  refers to the mesons  $\pi$  or  $\sigma_\pi$  while  $M_K$  refers to the mesons  $K$  or  $\sigma_K$  as required. The mesons  $\eta$  and  $\eta'$ , or correspondingly the scalars  $\sigma$  and  $\sigma'$  are coupled. Here the quark-antiquark scattering amplitude in either sector takes the matrix form

$$M = 2K(1 - 2\Pi K)^{-1} \quad (2.13)$$

where

$$\Pi = \begin{pmatrix} \Pi_{00} & \Pi_{08} \\ \Pi_{80} & \Pi_{88} \end{pmatrix} \quad (2.14)$$

with

$$\begin{aligned} \Pi_{00} &= \frac{1}{3}(2\Pi^{qq} + \Pi^{ss}) \\ \Pi_{08} = \Pi_{80} &= \frac{\sqrt{2}}{3}(\Pi^{qq} - \Pi^{ss}) \\ \Pi_{88} &= \frac{1}{3}(\Pi^{qq} + 2\Pi^{ss}) \end{aligned} \quad (2.15)$$

and

$$K = \begin{pmatrix} K_{00} & K_{08} \\ K_{80} & K_{88} \end{pmatrix}, \quad (2.16)$$

$$K_{ii} = K_i^\pm, K_{08} = K_{80} = \frac{1}{2}K_m^\pm \quad (2.17)$$

in either the scalar or pseudoscalar sector. For the purposes of our calculation of  $\pi K$  scattering lengths, we will not require information on the  $\eta$  and  $\eta'$  mesons. However, the exchange of a  $\sigma$  or  $\sigma'$  in the intermediate state within  $\pi K$  scattering may occur. We thus require the quark-antiquark scattering amplitude for the exchange of the  $\sigma$  and  $\sigma'$ . This can be written as

$$D_{\sigma,\sigma'} = M_{00}\lambda_0 \times \lambda_0 + M_{08}\lambda_0 \times \lambda_8 + M_{80}\lambda_8 \times \lambda_0 + M_{88}\lambda_8 \times \lambda_8 \quad . \quad (2.18)$$

Since the neutral  $\sigma$  and  $\sigma'$  are both exchanged in any single process, it is not necessary to resolve this scattering amplitude into the individual components for these particles via diagonalization. For our purposes, the individual masses and couplings are not required, although this provides an alternative method. The reader is referred to Refs. [9,20], who perform such a diagonalization explicitly.

### III. SCATTERING LENGTHS FOR $\pi K \rightarrow \pi K$ AT $T = 0$

In general, if one regards the process  $a + b \rightarrow a' + b'$ , the scattering amplitude for a fixed isospin  $I$  can be decomposed into partial wave amplitudes, *i.e.*

$$T^I(s, t, u) = 16\pi \sum_{l=0}^{\infty} (2l+1) t_l^I(s) P_l(\cos \theta) \quad (3.1)$$

where  $s$ ,  $t$  and  $u$  are the usual Mandelstam variables  $s = (p_a + p_b)^2$ ,  $t = (p_a - p_{a'})^2$  and  $u = (p_a - p_b')^2$ , and  $\theta$  is the scattering angle. The phases  $\delta_l(s)$  parametrize the scattering amplitude as

$$t_l^I(s) = \frac{\sqrt{s}}{2q} \frac{1}{2i} \left[ e^{2i\delta_l^I(s)} - 1 \right] \quad , \quad (3.2)$$

where

$$q = \frac{1}{2\sqrt{s}} \sqrt{[s - (m_a + m_b)^2][s - (m_a - m_b)^2]} \quad (3.3)$$

is the center of mass momentum of the incoming particles. The differential cross section is

$$\frac{d\sigma^I}{d\Omega} = \frac{1}{64\pi^2 s} |T^I(s, t)|^2 \quad , \quad (3.4)$$

while the total cross section can be expressed purely in terms of the phase shifts,

$$\sigma^I = \frac{4\pi}{q^2} \sum_l (2l + 1) \sin^2 \delta_l^I(s) \quad . \quad (3.5)$$

At low energies, the partial wave amplitudes can be expanded in the form

$$\Re [t_l^I(s)] = \frac{\sqrt{s}}{2} q^{2l} [a_l^I + b_l^I q^2 + O(q^4)] \quad , \quad (3.6)$$

defining the scattering amplitudes  $a_l^I$  and the slope parameters  $b_l^I$ . At the kinematic threshold  $q \rightarrow 0$ , the cross sections in each isospin channel are given purely in terms of the  $s$ -wave amplitudes, *i.e.*

$$\sigma^I = 4\pi (a_0^I)^2 \quad . \quad (3.7)$$

Our interest is in the  $\pi K$  system, and we start with the process of maximal isospin,  $I = 3/2$ ,

$$\pi^+ + K^+ \rightarrow \pi^+ + K^+ \quad . \quad (3.8)$$

By exchanging particles  $a$  and  $a'$ , one directly obtains the scattering process

$$\pi^- + K^+ \rightarrow \pi^- + K^+ \quad , \quad (3.9)$$

in which  $u$  is the center of mass variable. This reaction contains not only an  $I = 3/2$  component, but the  $I = 1/2$  component also. Crossing matrices relate the various amplitudes. Using an obvious notation, one may write

$$\begin{aligned}
T_s^I(s, t, u) &= \sum_{I'=1/2}^{3/2} C_{I,I'}^{su} T_u^{I'}(s, t, u) \\
&= C_{I,1/2}^{su} T_u^{1/2}(s, t, u) + C_{I,3/2}^{su} T_u^{3/2}(s, t, u) \quad ,
\end{aligned} \tag{3.10}$$

with the crossing matrix [23]

$$C_{I,I'}^{su} = \frac{1}{3} \begin{pmatrix} -1 & 4 \\ 2 & 1 \end{pmatrix} . \tag{3.11}$$

In practice, this tells us that

$$T^{1/2}(s, t, u) = \frac{3}{2} T^{3/2}(u, t, s) - \frac{1}{2} T^{3/2}(s, t, u) \tag{3.12}$$

so that the determination of scattering in the isospin channel  $I = 3/2$  is sufficient to obtain all information, including the amplitude in the  $T = 1/2$  channel. We therefore examine the process  $\pi^+ K^+ \rightarrow \pi^+ K^+$  in what follows.

### A. General Classification of Diagrams

Since the coupling strengths in the NJL model,  $G\Lambda^2$  and  $K\Lambda^5$  are large, a perturbative expansion in the coupling strengths is inadmissible. An alternative expansion in the inverse number of colors  $N_c$  is generally made [10,11]. In this expansion, fermion loops contribute a factor of  $N_c$ , while the scattering amplitudes with mesonic intermediate states contribute a factor of  $1/N_c$ . Thus the diagrams that are leading in the  $1/N_c$  expansion, and which are of the same order in this expansion, are both the box diagrams of the type displayed in Fig. 1 and the mesonic exchange graphs of Fig. 2.

### B. Contributions to $\pi^+ K^+ \rightarrow \pi^+ K^+$ .

### 1. Box diagrams

For the process  $\pi^+ K^+ \rightarrow \pi^+ K^+$ , only one of the box diagrams of Fig. 1 that is commensurate with isospin and strangeness conservation survives. This is depicted, together with the appropriate kinematic variables, in Fig. 3. A direct translation of this diagram leads to the expression

$$i T_{\text{box}} = -4(i g_{\pi q q})^2 (i g_{K s q})^2 N_c \quad (3.13)$$

$$\times \int \frac{d^4 q}{(2\pi)^4} \text{tr} [i \gamma_5 i S^q(q) i \gamma_5 i S^q(q - p_1) i \gamma_5 i S^q(q - k_2 + k_1) i \gamma_5 i S^s(q - k_2)] \quad .$$

Here the factor 4 arises from the flavor algebra. It has also been assumed that the translation of the Feynman graph gives  $i T$ .

### 2. Meson exchange graphs

As in the previous subsection, it is necessary to analyse first which diagrams can contribute to the  $\pi^+ K^+$  elastic scattering amplitude. One notes immediately that the  $s$  channel graphs of Fig. 2 do not contribute, due to charge conservation - the intermediate state would require a doubly charged (scalar) meson, which does not exist within the model. In the  $t$  channel, on the other hand, there are six possibilities. These are displayed explicitly in Fig. 4. Note that in all these diagrams, a scalar meson is exchanged in the intermediate channel. This is a consequence of parity conservation and manifests itself directly in the evaluation of the triangle diagrams that form a part of each amplitude in Fig. 4, in that the trace of the product of  $\gamma_5 S \gamma_5 S \gamma_5 S$  vanishes, whereas that of  $\gamma_5 S \gamma_5 S 1 S$  does not. We construct these diagrams by first considering the triangle graph that is given in Fig. 5. From this Feynman diagram, the three meson vertex is given as

$$-i \Gamma_1^{12}(k_1, k_2) = -N_c \int \frac{d^4 q}{(2\pi)^4} \text{tr} [i \gamma_5 i S^1(q) i \gamma_5 i S^2(q - k_1) i S^2(q - k_2)] \quad (3.14)$$

$$= -N_c \int \frac{d^4 q}{(2\pi)^4} \text{tr} \frac{i\gamma_5 i(\not{q} + m_1) i\gamma_5 i(\not{q} - k_1 + m_2) i(\not{q} - k_2 + m_2)}{(q^2 - m_1^2)[(q - k_1)^2 - m_2^2][(q - k_2)^2 - m_2^2]} \quad ,$$

where the superscripts 1 and 2 denote the flavors of the internal quarks and no trace over flavor has been included at this stage. This must be combined with the effective propagators of the scalar mesonic sector. We may simply use the form

$$D_{\sigma,\sigma'}(k_1 - k_2) = M_{00}\lambda_0 \times \lambda_0 + M_{08}\lambda_0 \times \lambda_8 + M_{80}\lambda_8 \times \lambda_0 + M_{88}\lambda_8 \times \lambda_8 \quad , \quad (3.15)$$

where the  $M_{ij}$  are a function of momenta,  $M_{ij} = M_{ij}(k_1 - k_2)$ . If, for example, a strange quark couples to the first vertex and a  $u$  quark to the second of the mesonic amplitude, as is the case in (c) and (d) of Fig. 4, one can obtain the flavor factors by considering the flavor components of Eq. (3.15) separately. The 8-0 term of this expression, for example, is thus

$$\begin{aligned} \lambda_8(s, s) \cdot \lambda_0(u, u) &= (001)\lambda_8 \begin{pmatrix} 0 \\ 0 \\ 1 \end{pmatrix} \cdot (100)\lambda_0 \begin{pmatrix} 1 \\ 0 \\ 0 \end{pmatrix} \\ &= -\frac{2\sqrt{2}}{3} \quad , \end{aligned} \quad (3.16)$$

and the other terms follow similarly, leading to the expression

$$D_{\sigma,\sigma'}^{qs} = \frac{2}{3}M_{00} - \frac{\sqrt{2}}{3}M_{08} - \frac{2}{3}M_{88} \quad . \quad (3.17)$$

This form of the intermediate mesonic scattering amplitude is required for the evaluation of diagrams (c) and (d). With it, one easily constructs the  $t$  channel  $\pi K$  scattering amplitudes in (c) and (d) to be

$$iT_{t,\{(c)+(d)\}}^{3/2}(k_1, k_2, p_1, p_2) = -i2 \cdot 4g_{\pi qq}^2 g_{Ksq}^2 \Gamma_1^{qs}(k_1, k_2) D_{\sigma,\sigma'}^{sq}(k_1 - k_2) \Gamma_1^{qq}(-p_2, -p_1) \quad , \quad (3.18)$$

since terms (c) and (d) are equal when  $m_u = m_d$ . In this expression, the factor 4 arises from the external vertices, that each contribute a factor  $\sqrt{2}$ . The factor 2 comes about since the contributions from graphs (c) and (d) are equal.

In an analogous fashion, diagrams (a) and (b) can also be evaluated. The intermediate mesonic scattering amplitude in this case is found to be

$$D_{\sigma,\sigma'}^{qq}(k_1 - k_2) = \frac{2}{3}M_{00} + \frac{2\sqrt{2}}{3}M_{08} + \frac{1}{3}M_{88} \quad , \quad (3.19)$$

and in combination with Eq. (3.14) leads to the expression

$$iT_{t,\{(a)+(b)\}}^{3/2}(k_1, k_2, p_1, p_2) = -i2 \cdot 4g_{\pi qq}^2 g_{Kqs}^2 \Gamma_1^{sq}(-k_2, -k_1) D_{\sigma,\sigma'}^{qq}(k_1 - k_2) \Gamma_1^{qq}(p_1, p_2) \quad (3.20)$$

for the  $t$  channel  $\pi^+ K^+$  scattering amplitudes depicted in (a) and (b).

There is no contribution from diagrams (e) and (f): the only difference between these two graphs is seen to be due to the flavor couplings to the intermediate exchanged meson  $\sigma_\pi$ . Since  $\lambda_3(u, u) = -\lambda_3(d, d)$ , the sum of these two terms cancel, and hence

$$iT_{t,\{(e)+(f)\}}^{3/2} = 0 \quad . \quad (3.21)$$

Thus, in the  $t$  channel, the  $\pi^+ K^+$  amplitude leads to

$$T_t^{3/2} = T_{t,\{(a)+(b)\}}^{3/2} + T_{t,\{(c)+(d)\}}^{3/2} \quad , \quad (3.22)$$

with  $T_{t,\{(a)+(b)\}}^{3/2}$  and  $T_{t,\{(c)+(d)\}}^{3/2}$  as given in Eqs. (3.20) and (3.18).

We now come to the  $u$  channel graphs of Fig. 2. Such processes require the exchange of an uncharged strange meson. In the NJL model, this corresponds to the exchange of a  $\sigma_K$  and can be realized within the model as depicted in Fig. 6. An elementary vertex needed for this process is shown in Fig. 7. Analytically, it can be constructed as

$$\begin{aligned} -i\Gamma_2^{12}(k_1, p_2) &= -N_c \int \frac{d^4 q}{(2\pi)^4} \text{tr}[i\gamma_5 iS^1(q) i\gamma_5 iS^2(q - k_1) iS^1(q - p_2)] \quad (3.23) \\ &= -N_c \int \frac{d^4 q}{(2\pi)^4} \text{tr} \frac{i\gamma_5 i(\not{q} + m_1) i\gamma_5 i(\not{q} - \not{k}_1 + m_2) i(\not{q} - \not{p}_2 + m_1)}{(q^2 - m_1^2)[(q - k_1)^2 - m_2^2][(q - p_2)^2 + m_1^2]} \end{aligned}$$

while the effective interaction mediated by the  $\sigma_K$  meson follows from Eq. (2.9) as

$$D_{\sigma_K}(k_1 - p_2) = \frac{2K_{44}^-}{1 - 2K_{44}^- \Pi_{sq}^S(k_1 - p_2)} \quad , \quad (3.24)$$

so that one arrives at the form

$$iT_u^{3/2}(k_1, k_2, p_1, p_2) = -8ig_{\pi qq}^2 g_{Ksq}^2 \Gamma_2^{qs}(k_1, p_2) D_{\sigma_K}(k_1 - p_2) \Gamma_2^{qs}(k_2, p_1) \quad (3.25)$$

for the  $u$  channel amplitude. The factor  $8(= \sqrt{2}^6)$  in this expression comes from all flavor factors that contribute at each vertex.

The complete  $I = 3/2$   $\pi^+ K^+ \rightarrow \pi^+ K^+$  scattering amplitude is thus made up of three components,

$$T^{3/2}(k_1, k_2, p_1, p_2) = T_{\text{box}}^{3/2}(k_1, k_2, p_1, p_2) + T_t^{3/2}(k_1, k_2, p_1, p_2) + T_u^{3/2}(k_1, k_2, p_1, p_2) \quad , \quad (3.26)$$

with  $T^{\text{box}}$ ,  $T_t^{3/2}$  and  $T_u^{3/2}$  given by Eqs. (3.13), (3.22) and (3.25) respectively.

### C. $\pi K$ scattering lengths

The expressions given in the previous section enable one in principle to calculate the  $\pi K$  cross section for an arbitrary choice of kinematic variables. In practice, this turns out to be extremely difficult, as the box diagram cannot easily be evaluated exactly for arbitrary kinematics, requiring in general additional approximations. In this paper, we restrict ourselves to a calculation of the scattering lengths, which simplifies the calculation somewhat. The kinematic threshold is given by

$$s = (m_\pi + m_K)^2 \quad (3.27)$$

with

$$t = 0, \quad u = (m_\pi - m_K)^2, \quad q = 0 \quad . \quad (3.28)$$



These conditions can be fulfilled by choosing

$$k_1 = k_2 = k = \begin{pmatrix} m_K \\ \vec{0} \end{pmatrix} \quad (3.29)$$

and

$$p_1 = p_2 = p = \begin{pmatrix} m_\pi \\ \vec{0} \end{pmatrix} . \quad (3.30)$$

Using these kinematics, the box term, as well as the triangle and intermediate meson exchange graphs making up the  $t$  and  $u$  channel contributions, can be expressed in terms of the “elementary” integrals

$$F^i = \int \frac{d^4q}{(2\pi)^4} \frac{1}{q^2 - m_i^2} \quad (3.31)$$

$$M^{12}(p) = \int \frac{d^4q}{(2\pi)^4} \frac{1}{(q^2 - m_1^2)[(q-p)^2 - m_2^2]} \quad (3.32)$$

$$N^{12}(p) = \int \frac{d^4q}{(2\pi)^4} \frac{1}{(q^2 - m_1)^2[(q-p)^2 - m_2^2]} \quad (3.33)$$

$$P^{12}(p, k) = \int \frac{d^4q}{(2\pi)^4} \frac{1}{(q^2 - m_1^2)[(q-p)^2 - m_1^2][(q-k)^2 - m_2^2]} \quad (3.34)$$

$$Q^{12}(p, k) = \int \frac{d^4q}{(2\pi)^4} \frac{1}{(q^2 - m_1^2)^2[(q-p)^2 - m_1^2][(q-k)^2 - m_2^2]} \quad (3.35)$$

that form the building blocks for these functions. We list the results for the components of the  $T^{3/2}$  amplitude for the threshold kinematics.

### 1. Box diagram

The kinematic choice of Eqs. (3.29) and (3.30) lead to the forms

$$i T_{\text{box}}^{3/2}(k, k, p, p) = -4N_c g_{\pi qq}^2 g_{Kqs}^2 \quad (3.36)$$

$$\times \int \frac{d^4q}{(2\pi)^4} \left\{ \frac{\text{tr} [\gamma_5(\not{q} - \not{k} + m_s)\gamma_5(\not{q} + m_q)\gamma_5(\not{q} - \not{p} + m_q)\gamma_5(\not{q} + m_q)]}{[(q-k)^2 - m_s^2][q^2 - m_q^2]^2[(q-p)^2 - m_q^2]} \right\} .$$

After some calculation along the lines that will be indicated for the three meson vertex function to follow, one finds

$$\begin{aligned}
iT_{\text{box}}^{3/2}(k, k, p, p) = & -8g_{\pi qq}^2 g_{Kqs}^2 N_c \left\{ M^{qq}(0) + M^{qs}(k-p) - p^2 N^{qq}(p) \right. \\
& - \left[ k^2 - (m_q - m_s)^2 \right] N^{qs}(k) - 2k \cdot p P^{qs}(p, k) \\
& \left. + p^2 \left[ k^2 - (m_q - m_s)^2 \right] Q^{qs}(p, k) \right\} . \quad (3.37)
\end{aligned}$$

## 2. Meson exchange graphs

The three meson vertex functions are required for the  $t$  and  $u$  channel graphs. From Eq. (3.14), one has

$$-i\Gamma_1^{12}(k, k) = -iN_c \int \frac{d^4q}{(2\pi)^4} \frac{\text{tr} [\gamma_5 (\not{q} + \not{k} + m_1) \gamma_5 (\not{q} + m_2) (\not{q} + m_2)]}{[q^2 - m_2^2]^2 [(q+k)^2 - m_1^2]} , \quad (3.38)$$

which reduces to

$$-i\Gamma_1^{12}(k, k) = -4iN_c \int \frac{d^4q}{(2\pi)^4} \frac{q^2(m_1 - 2m_2) - 2m_2 q \cdot k + m_1 m_2^2}{(q^2 - m_2^2)^2 [(q+k)^2 - m_1^2]} , \quad (3.39)$$

after performing the trace. Using the relation

$$2k \cdot q = [(k+q)^2 - m_1^2] - [q^2 - m_2^2] - k^2 - m_2^2 + m_1^2 \quad (3.40)$$

leads one to the expression

$$\begin{aligned}
-i\Gamma_1^{12}(k, k) = & -4iN_c \left\{ -m_2 M^{22}(0) + (m_1 - m_2) M^{21}(k) \right. \\
& \left. + m_2 [k^2 - (m_2 - m_1)^2] N^{21}(k) \right\} \quad (3.41)
\end{aligned}$$

in terms of the elementary integrals. In a similar fashion, the second vertex function that is required for the  $u$  channel  $T$  matrix amplitude of Eq. (3.23) and which was shown in Fig. 7 can be decomposed as

$$\begin{aligned}
-i\Gamma_2^{12}(k, p) &= 2N_c i \left\{ (m_2 - m_1)M^{12}(k) + (m_2 + m_1)M^{12}(k - p) \right. \\
&\quad \left. - [m_2 p^2 + m_1 k^2 - m_1(p - k)^2]P^{12}(p, k) \right\} . \quad (3.42)
\end{aligned}$$

In addition to this, the scalar polarization function is given as

$$-i\Pi_S^{12}(k) = -2N_c \int \frac{d^4q}{(2\pi)^4} \frac{\text{tr}[i(\not{q} + m_1)i(\not{q} - \not{k} + m_2)]}{[q^2 - m_1^2][(q - k)^2 - m_2^2]} , \quad (3.43)$$

and is expressed as

$$-i\Pi_S^{12}(k) = 4N_c \{F^1 + F^2 + [(m_1 + m_2)^2 - k^2]M^{12}(k)\} . \quad (3.44)$$

Note that the pseudoscalar polarization differs from this function only in the replacement  $(m_1 + m_2)^2 \rightarrow (m_1 - m_2)^2$ .

The complete expression for the  $I = 3/2$  scattering amplitude at the kinematic threshold follows now on constructing

$$iT_{t\{(a)+(b)\}}^{3/2}(k, k, p, p) = -8ig_{\pi qq}^2 g_{Kqs}^2 \Gamma_1^{sq}(k, k) \left( \frac{2}{3}M_{00} + \frac{2\sqrt{2}}{3}M_{08} + \frac{1}{3}M_{88} \right) \Gamma_1^{qq}(p, p) \quad (3.45)$$

and

$$iT_{t\{(c)+(d)\}}^{3/2}(k, k, p, p) = -8ig_{\pi qq}^2 g_{Kqs}^2 \Gamma_1^{qs}(k, k) \left( \frac{2}{3}M_{00} - \frac{\sqrt{2}}{3}M_{08} - \frac{2}{3}M_{88} \right) \Gamma_1^{qq}(p, p) \quad (3.46)$$

for the  $t$  channel, and

$$iT_u^{-2}(k, k, p, p) = -8ig_{\pi qq}^2 g_{Kqs}^2 [\Gamma_2^{qs}(k, p)]^2 \frac{2K_{44}^-}{1 - 2K_{44}^- \Pi_S^{qs}(k - p)} \quad (3.47)$$

for the  $u$  channel, with the couplings

$$\begin{aligned}
g_{Kqs}^{-2} &= -4iN_c \left\{ M^{qs}(k) + \frac{(m_q - m_s)^2 - k^2}{2k^2} [M^{qs}(k) - M^{ss}(0)] \right. \\
&\quad \left. + (m_s^2 - m_q^2 + k^2)N^{sq}(k) \right\}_{k^2=m_K^2} \quad (3.48)
\end{aligned}$$

and

$$g_{\pi qq}^{-2} = -2iN_c \left[ M^{qq}(0) + M^{qq}(k) - k^2 N^{qq}(k) \right]_{k^2=m_\pi^2}, \quad (3.49)$$

which can be derived from the definitions in Eq. (2.12). Then one has

$$\begin{aligned} T^{3/2}(k, k, p, p) &= T_{\text{box}}^{3/2}(k, k, p, p) + T_{t\{(a)+(b)\}}^{3/2}(k, k, p, p) \\ &+ T_{t\{(c)+(d)\}}^{3/2}(k, k, p, p) + T_u^{3/2}(k, k, p, p) \quad . \end{aligned} \quad (3.50)$$

The scattering lengths are evaluated as

$$a^I = \frac{1}{8\pi(m_\pi + m_K)} \Re \left[ T^I(s = (m_\pi + m_K)^2, t = 0, u = (m_\pi - m_K)^2) \right] \quad , \quad (3.51)$$

so that  $a^{3/2}$  follows directly from Eq. (3.50), while  $a^{1/2}$  is obtained subsequently through the relation Eq. (3.12).

## IV. NUMERICAL EVALUATION OF THE $\pi K$ SCATTERING LENGTHS

### A. $T=0$ Case

In order to evaluate the scattering lengths, the functions  $F$ ,  $M$ ,  $N$ ,  $P$  and  $Q$  of Eqs. (3.31) - (3.35) must be evaluated. Since the NJL model is non-renormalizable, a cutoff parameter must be introduced to regulate these functions. This can be done in a covariant fashion using the Pauli-Villars scheme, or non-covariantly by introducing a cutoff on the three momentum  $|\vec{p}| < \Lambda_3$ . For consistency, a cutoff is included in all integrals, including  $N$ ,  $P$  and  $Q$ , that are convergent. Technical details for the Pauli-Villars integrals are given in Appendix A. The  $O(3)$  calculation is performed directly numerically. Our first evaluation is performed at  $T = 0$ .

In Table I, we list two sets of parameters for the Pauli-Villars calculation that were taken from Ref. [19], as well as two sets of parameters for an  $O(3)$  cutoff, taken

from Refs. [9,20]. These calculations are all non-chiral, all assuming non-vanishing values for the current quark masses. Using these parameter sets, we obtain values for the pseudoscalar meson sector at  $T = 0$  that are listed in Table II. The experimental values are also given. The scalar meson masses for  $T = 0$  for the corresponding parameter sets are given in Table III. Using these values, the  $s$ -wave scattering lengths  $a_0^{1/2}$  and  $a_0^{3/2}$  are calculated at  $T = 0$ . The results for  $a_0^{3/2}$ , obtained from the box,  $t$  and  $u$  channels for each parameter set, are given in Table IV, with those for  $a_0^{1/2}$  given in Table V. The final results for the scattering lengths arise from a delicate cancellation of the box,  $t$  and  $u$  channel values, which is evident from these tables<sup>3</sup>. In the model, we find that the calculated values of  $a_0^{3/2}$  range from  $-0.003$  to  $-0.04$ , while that of  $a_0^{1/2}$  range from  $0.13$  to  $0.18$ , in units of  $m_\pi$ . Our results for  $a_0^{1/2}$  fall well within the experimentally known range of  $0.13$  to  $0.24$ , while those for  $a_0^{3/2}$  are lower, the experimental values being  $-0.13$  to  $-0.05$ . Standard chiral perturbation theory gives  $a_0^{1/2} = 0.17$  and  $a_0^{3/2} = -0.05$  [1] for these values. Thus our  $T = 0$  values, while dependent on the regularization scheme, can be considered reasonable.

### B. $\pi K$ scattering lengths for $T \neq 0$

At finite values of the temperature, the  $\pi K$  scattering graphs can be analysed as was done at  $T = 0$ , but within the imaginary time or Matsubara formalism. This corresponds to making the formal substitution

---

<sup>3</sup>To obtain a deeper understanding of this fact, it is necessary to perform a chiral expansion of the box,  $s$ ,  $t$  and  $u$  channel graphs in the two variables ( $m_\pi/\Lambda$  and  $m_K/\Lambda$ ) analytically along the lines suggested by Refs [17] and [18]. This is a difficult problem in its own right and will not be addressed here.

$$\int \frac{d^4 q}{(2\pi)^4} \rightarrow \frac{i}{\beta} \sum_n \int_{\Lambda} \frac{d^3 q}{(2\pi)^3} \quad (4.1)$$

and replacing the fermionic (bosonic)  $q_0$  by the discrete frequencies  $i\omega_n$ ,  $\omega_n = (2n + 1)\pi/\beta$  or  $\omega_n = 2n\pi/\beta$ ,  $n = 0, \pm 1, \pm 2, \pm 3 \dots$  respectively. The final expressions are given in Appendix B. As is indicated in Eq. (4.1), an  $O(3)$  cutoff is naturally implemented.

The pseudoscalar meson pole masses vary with temperature, and this variation is shown in Fig. 8, together with the dissociation threshold for the kaon,  $m_q + m_s$ , which leads to a kaon dissociation temperature  $T_{MK}$ . The function  $m_K + m_\pi$  is also shown. The temperature at which this function crosses  $m_q + m_s$  defines the point  $T_{\pi K}$  at which a meson pair can dissociate into a quark pair. Numerically, for the set of parameters denoted as HK in Table I, we have  $T_{\pi K} = 174.5$  MeV, while  $T_{MK} = 203.0$  MeV. We also show the temperature dependence of the scalar mesonic sector in Fig. 9 for this parameter set. Note that the behavior of the  $\sigma_\pi$  meson with temperature [20] has been confirmed qualitatively in lattice gauge calculations [13]. Using the temperature dependent functions for the mesons, the temperature dependence of the box,  $t$  and  $u$  channel amplitudes is evaluated and used to construct the scattering lengths. In Fig. 10, we show the individual contributions from these channels, together with the evaluated scattering length  $a_0^{3/2}$ . One sees that all graphs diverge close to the Mott point. The box and  $u$  channel graphs do not change substantially up until the Mott point, while the  $t$  channel meson exchange diagram displays a somewhat faster variation with temperature. Consequently, the resulting change in  $a_0^{3/2}$  is noticeable - the change, within this model calculation, is quantitatively given as  $a_0^{3/2}(T = 150 \text{ MeV})/a_0^{3/2}(T = 0) = 2.36$ , in contrast to the completely flat temperature dependence found for  $\pi\pi$  scattering lengths [21]. The temperature dependence of the  $a_0^{1/2}$  is less dramatic: Fig. 11 shows that the sum of the functional components lead to a flat behavior. Quantitatively, one has

$$a_0^{1/2}(T = 150 \text{ MeV})/a_0^{1/2}(T = 0) = 1.18.$$

## V. SUMMARY AND CONCLUSIONS

In this paper, we have evaluated the temperature dependence of the  $\pi K$  scattering lengths  $a_0^{3/2}$  and  $a_0^{1/2}$  within the framework of the SU(3) NJL model. Ordering terms according to an expansion in  $1/N_c$  is used to determine the leading set of diagrams that contribute to the scattering amplitude. One finds a box-like graph, as well as  $t$  and  $u$  channel graphs. To this order in  $N_c$ , no unitarity corrections are present. Because of this, only the scattering lengths are investigated, although the formulae are given for arbitrary kinematics, so that the scattering amplitude can be evaluated for arbitrary kinematics. The restriction here to threshold kinematics also simplifies the computation considerably.

At  $T = 0$ , we have calculated the  $l = 0$  scattering lengths  $a_0^{1/2}$  and  $a_0^{3/2}$  for different regularization schemes, that of Pauli and Villars, and also using an O(3) cutoff. We have simply used parameters sets of other authors and have not fitted any additional quantities. We find that  $a_0^{1/2}$  falls well within the experimentally known data bracket, while  $a_0^{3/2}$  is slightly lower than the bracketing values given experimentally. Unfortunately the experimental values are not known precisely at this stage.

In investigating the finite temperature behavior of the scattering amplitudes, we observe that the box and  $u$  channel graphs, the latter of which occurs by resonance exchange of a  $\sigma_K$  scalar meson, do not vary strongly with the temperature. However, variation of the  $t$  channel amplitude that is controlled by the exchange of  $\sigma$  and  $\sigma'$  mesons displays a slightly more pronounced temperature dependence, leading to a temperature change of  $a_0^{3/2}$  of a factor of about 2 over 150 MeV. This is in contrast to the case for  $\pi\pi$  scattering, in which the  $\pi\pi$  scattering lengths are found to be

essentially independent of temperature over a range of about 150 MeV. The study of kaon physics appears here to give a stronger functional dependence than in the pionic case. Since this is driven essentially by the temperature dependence of the intermediate scalar mesons, it seems that processes that involve the exchange of mesons in the scalar sector may ultimately provide us with a clean signal for a chiral phase transition.

### ACKNOWLEDGMENTS

This work has been supported in part by the Deutsche Forschungsgemeinschaft DFG under the contract number Hu 233/4-4, and by the German Ministry for Education and Research (BMBF) under contract number 06 HD 742. One of us (S.P.K.) would like to thank S. Kahana for the generous hospitality at Brookhaven National Laboratory, where this paper was written.

### APPENDIX A: PAULI-VILLARS REGULARIZATION

Standard Feynman parametrization [24],

$$\prod_{i=1}^n \frac{1}{A_i^{\zeta_i}} = \frac{\Gamma(\zeta)}{\prod_{i=1}^n \Gamma(\zeta_i)} \int_0^1 \left( \prod_{i=1}^n dx_i x_i^{\zeta_i-1} \right) \frac{\delta(1-x)}{(\sum_{i=1}^n x_i A_i)^{\zeta}} \quad , \quad (\text{A1})$$

with  $\zeta = \sum_{i=1}^n \zeta_i$  and  $x = \sum_{i=1}^n x_i$  is used for the integrals Eqs. (3.31)–(3.35). All calculations are performed at the kinematic threshold. One has

$$F = \int \frac{d^4 q}{(2\pi)^4} \frac{1}{q^2 - m^2} \quad , \quad (\text{A2})$$

which, after Wick rotation, gives

$$F = -\frac{i}{(4\pi)^2} \left[ q^2 - m^2 \ln |q^2 + m^2| \right]_0^\infty \quad . \quad (\text{A3})$$

The Pauli-Villars regularization scheme is then implemented:



$$\begin{aligned}
F &= -\frac{i}{(4\pi)^2} \sum_{j=0}^2 C_j \left[ (m^2 + \alpha_j \Lambda^2) \ln |q^2 + m^2 + \alpha_j \Lambda^2| \right]_0^\infty \\
&= -\frac{im^2}{(4\pi)^2} \left[ \ln \left| 1 - \left( \frac{m^2}{\Lambda^2} + 1 \right)^{-2} \right| + 2 \frac{\Lambda^2}{m^2} \ln \left| 1 + \left( \frac{m^2}{\Lambda^2} + 1 \right)^{-1} \right| \right] , \quad (\text{A4})
\end{aligned}$$

where  $m_j = m^2 + \alpha_j \Lambda^2$  and the standard set of parameters  $C_0 = 1$ ,  $C_1 = 1$ ,  $C_2 = -2$ ,  $\alpha_0 = 0$ ,  $\alpha_1 = 2$  and  $\alpha_2 = 1$  are used.

The function  $M^{12}(p)$  from Eq. (3.32) can be integrated after Wick rotation. One has

$$\begin{aligned}
M^{12}(p) &= i \int \frac{d^4 q_E}{(2\pi)^4} \int_0^1 dx \frac{1}{(q^2 + R^2)^2} \\
&= \frac{i}{(4\pi)^2} \int_0^1 dx \left[ \frac{R^2}{q^2 + R^2} + \ln(q^2 + R^2) \right]_0^\infty \quad (\text{A5})
\end{aligned}$$

with  $R^2 = m_1^2 x + m_2^2(1-x) - p^2(1-x)x$ . The Pauli-Villars regularized version reads

$$M^{12}(p) = \frac{i}{(4\pi)^2} \sum_{j=0}^2 C_j \int_0^1 dx \left[ \frac{R_j^2}{q^2 + R_j^2} + \ln(q^2 + R_j^2) \right]_0^\infty , \quad (\text{A6})$$

with the replacements  $m_1^2 \rightarrow m_{1j}^2 = m_1^2 + \alpha_j \Lambda^2$  and  $m_2^2 \rightarrow m_{2j}^2 = m_2^2 + \alpha_j \Lambda^2$  in  $R^2$  defining  $R_j^2$ . One obtains

$$M^{12}(p) = -\frac{i}{(4\pi)^2} \sum_{j=0}^2 C_j \int_0^1 dx \ln \left[ \frac{(m_1^2 - m_2^2)x + m_{2j}^2 - p^2(1-x)x}{m_2^2} \right] . \quad (\text{A7})$$

The  $x$ -integration can be performed explicitly leading to

$$M^{12}(p) = -\frac{i}{(4\pi)^2} \sum_{j=0}^2 C_j \left[ \ln \frac{m_{2j}^2}{m_2^2} + \frac{p^2 + m_1^2 - m_2^2}{2p^2} \ln \left( \frac{m_{1j}^2}{m_{2j}^2} \right) + \frac{1}{p^2} A_j \right] , \quad (\text{A8})$$

with  $\Delta_j = (m_1^2 - m_2^2 - p^2)^2 - 4m_{2j}^2 p^2$  and

$$A_j = \sqrt{-\Delta_j} \left[ \tan^{-1} \left( \frac{p^2 + m_1^2 - m_2^2}{\sqrt{-\Delta_j}} \right) - \tan^{-1} \left( \frac{-p^2 + m_1^2 - m_2^2}{\sqrt{-\Delta_j}} \right) \right] \quad (\text{A9})$$

if  $\Delta_j < 0$  and

$$A_j = \sqrt{\Delta_j} \left[ \frac{1}{2} \ln \frac{p^2 - m_{1j}^2 - m_{2j}^2 + \sqrt{\Delta_j}}{p^2 - m_{1j}^2 - m_{2j}^2 - \sqrt{\Delta_j}} - i\pi \Theta \left( p^2 - (m_1 - m_2)^2 \right) \right] \quad (\text{A10})$$

if  $\Delta_j > 0$ . Following the same prescription for  $N^{12}(p)$  leads to

$$\begin{aligned} N^{12}(p) &= -\frac{i}{(4\pi)^2} \int_0^1 dx \frac{x}{R^2} \\ &= -\frac{i}{(4\pi)^2} \frac{1}{2p^2} \left[ \ln \left( \frac{m_1^2}{m_2^2} \right) + 2 \frac{m_1^2 - m_2^2 - p^2}{\Delta} A \right] . \end{aligned} \quad (\text{A11})$$

Both  $P^{12}(p, k)$  and  $Q^{12}(p, k)$  of Eqs. (3.34) and (3.35) are functions of two variables and are somewhat more complicated. Feynman parametrization followed by a Wick rotation and integration over the momentum variable leads to

$$P^{12}(p, k) = -\frac{i}{(4\pi)^2} \int_0^1 dx \int_0^1 dy \frac{y}{\hat{R}^2} \quad (\text{A12})$$

where

$$\hat{R}^2 = m_1^2(1 - y + xy) + m_2^2(1 - x)y - [k^2(1 - x) + p^2x]y(1 - y) - x(1 - x)y^2u , \quad (\text{A13})$$

with  $u = (p - k)^2$ . The integral in  $x$  can again be performed. One finds

$$P^{12}(p, k) = -\frac{2i}{(4\pi)^2} \int_0^1 \frac{dy}{\sqrt{\hat{\Delta}}} \left[ \tan^{-1} \left( \frac{2uy + \rho - \kappa y}{\sqrt{\hat{\Delta}}} \right) - \tan^{-1} \left( \frac{\rho - \kappa y}{\sqrt{\hat{\Delta}}} \right) \right] . \quad (\text{A14})$$

where the discriminant in this case is

$$\begin{aligned} -y^2\hat{\Delta} &= (\rho y - \kappa y^2)^2 - 4(m_1^2 + \omega y + k^2 y^2)y^2u \\ &= -y^2 \left[ (4m_1^2 u - \rho^2) + (2\rho\kappa + 4\omega u)y - (\kappa^2 - 4k^2 u)y^2 \right] , \end{aligned} \quad (\text{A15})$$

with  $\rho = m_1^2 - m_2^2 + k^2 - p^2$ ,  $\kappa = k^2 + u - p^2$  and  $\omega = m_2^2 - m_1^2 - k^2$ .

A similar analysis leads to

$$Q^{12}(p, k) = \frac{i}{(4\pi)^2} \int_0^1 \int_0^1 dx dy \frac{y(1 - y)}{(\hat{R}^2)^2} , \quad (\text{A16})$$

in which the  $x$  integration can once more be carried out with the aid of the integral

$$\int_0^1 \frac{dx}{[ax^2 + bx + c]^2} = -\frac{1}{\Delta} \left[ \frac{2ax + b}{ax^2 + bx + c} + \frac{4a}{\sqrt{-\Delta}} \tan^{-1} \left( \frac{2ax + b}{\sqrt{-\Delta}} \right) \right]_0^1 \quad (\text{A17})$$

with  $\Delta = b^2 - 4ac$ . Note that the Pauli-Villars regularization procedure has not been carried out explicitly on  $N^{12}(p)$ ,  $P^{12}(k, p)$  and  $Q^{12}(k, p)$ , which are convergent. For consistency within the model, however, this should be done. The implementation is simple. The standard replacement of each integral by a sum of three terms with  $C_j$  and  $m_{ji}$  is constructed and evaluated numerically. The forms for  $P$  and  $Q$ , Eqs.(A14) and (A17) are valid in the case that the integrands are non-singular.

## APPENDIX B: FINITE TEMPERATURE INTEGRALS

Using the abbreviation  $E_j^2 = q^2 + m_j^2$  for the energy of particle with flavor  $j$ , one finds the following forms for the integrals Eqs. (3.31) – (3.35) at the kinematic threshold:

$$F^j = -\frac{i}{4\pi^2} \int_0^\Lambda dq \frac{q^2}{E_j} \tanh\left(\frac{\beta E_j}{2}\right) \quad (\text{B1})$$

while

$$\begin{aligned} M^{12}(p) = & -\frac{i}{16\pi^2} \frac{1}{p_0^2} \left\{ \mathcal{P} \int dq \frac{q^2}{q_0^2 - q^2} \left[ \tanh\left(\frac{\beta E_1}{2}\right) \frac{p_0^2 + m_1^2 - m_2^2}{E_1} \right. \right. \\ & \left. \left. + \tanh\left(\frac{\beta E_2}{2}\right) \frac{p_0^2 + m_2^2 - m_1^2}{E_2} \right] \right. \\ & \left. -i \frac{\pi q_0}{2} \left[ \tanh\left(\frac{\beta E_{10}}{2}\right) \frac{q_0^2 + m_1^2 - m_2^2}{E_{10}} \right. \right. \\ & \left. \left. + \tanh\left(\frac{\beta E_{20}}{2}\right) \frac{q_0^2 + m_2^2 - m_1^2}{E_{20}} \right] \Theta(q_0^2) \right\} \quad (\text{B2}) \end{aligned}$$

where we have abbreviated

$$q_0^2 = \frac{[p_0^2 - (m_1 + m_2)^2][p_0^2 - (m_1 - m_2)^2]}{4p_0^2} \quad (\text{B3})$$

$$E_{j0} = \sqrt{q_0^2 + m_j^2} \quad . \quad (\text{B4})$$

For  $N^{12}(p)$  we find

$$\begin{aligned}
N^{12}(p) = & \frac{i}{32\pi^2} \frac{1}{p_0^4} \int_0^\Lambda dq \frac{q^2}{(q_0^2 - q^2)^2} \\
& \times \left[ \tanh\left(\frac{\beta E_1}{2}\right) \frac{(\xi + 2E_1^2)(\xi^2 + 4E_1^2 p_0^2) - 16\xi E_1^2 p_0^2}{4E_1^3} \right. \\
& - \tanh\left(\frac{\beta E_2}{2}\right) \frac{(p_0^2 - m_1^2 + m_2^2)^2 + 4p_0^2 E_2^2}{2E_2} \\
& \left. - \frac{\beta}{\cosh^2\left(\frac{\beta E_1}{2}\right)} \frac{p_0^2 (q_0^2 - q^2) (p_0^2 + m_1^2 - m_2^2)}{2E_1^2} \right] \quad (B5)
\end{aligned}$$

with  $\xi = p_0^2 + m_1^2 - m_2^2$ . For the function  $P^{12}(k, p)$  one has

$$P^{12}(p, k) = -\frac{i}{4\pi^2} \int_0^\Lambda dq \frac{q^2}{\delta_p \delta_k \delta_u} \left[ \tanh\left(\frac{\beta E_1}{2}\right) \frac{\mathcal{A}\delta_u + \mathcal{B}\delta_k}{E_1} + \tanh\left(\frac{\beta E_2}{2}\right) \frac{\mathcal{C}\delta_p}{E_2} \right] \quad (B6)$$

with

$$\delta_p = p_0^2 (p_0^2 - 4E_1^2) \quad (B7)$$

$$\delta_k = \left[ (k_0^2 + m_1^2 - m_2^2)^2 - 4E_1^2 k_0^2 \right] = \left[ (k_0^2 - m_1^2 + m_2^2)^2 - 4E_2^2 k_0^2 \right] \quad (B8)$$

$$\delta_u = \left[ (u + m_1^2 - m_2^2)^2 - 4E_1^2 u \right] = \left[ (u - m_1^2 + m_2^2)^2 - 4E_2^2 u \right] \quad (B9)$$

$$\mathcal{A} = \left[ p_0^2 (k_0^2 + m_1^2 - m_2^2) + 2E_1^2 (p_0^2 + k_0^2 - u) \right] \quad (B10)$$

$$\mathcal{B} = \left[ p_0^2 (u + m_1^2 - m_2^2) + 2E_1^2 (p_0^2 - k_0^2 + u) \right] \quad (B11)$$

$$\mathcal{C} = \left[ (k_0^2 - m_1^2 + m_2^2) (u - m_1^2 + m_2^2) - 2E_2^2 (p_0^2 - k_0^2 - u) \right] \quad (B12)$$

For the function  $Q^{12}(k, p)$ , one has

$$\begin{aligned}
Q^{12}(p, k) = & \frac{i}{4\pi^2} \int_0^\Lambda dq q^2 \left\{ \tanh\left(\frac{\beta E_1}{2}\right) \frac{\mathcal{D}}{2E_1^3 \delta_p^2 \delta_k^2} - \tanh\left(\frac{\beta E_1}{2}\right) \frac{\mathcal{E}}{E_1 \delta_p^2 \delta_u} \right. \\
& \left. - \tanh\left(\frac{\beta E_2}{2}\right) \frac{\mathcal{F}}{E_2 \delta_k^2 \delta_u} - \frac{\beta}{4 \cosh^2\left(\frac{\beta E_1}{2}\right)} \frac{\mathcal{G}}{E_1^2 \delta_p \delta_k} \right\} \quad (B13)
\end{aligned}$$

where

$$\begin{aligned}
\mathcal{D} = & p_0^2 \left[ \eta (2E_1^2 + p_0^2) + 2E_1^2 (4p_0^2 + 3k_0^2 - 3u) \right] \\
& \times \left[ (p_0^2 + 4E_1^2) (\eta^2 + 4k_0^2 E_1^2) + 8\eta E_1^2 (p_0^2 + k_0^2 - u) \right] \\
& - 4E_1^2 \left[ 2p_0^2 \eta + (p_0^2 + k_0^2 - u) (E_1^2 + p_0^2) + 2p_0^2 E_1^2 \right]
\end{aligned}$$

$$\times \left[ 2p_0^2 (\eta^2 + 4k_0^2 E_1^2) + \eta (p_0^2 + k_0^2 - u) (p_0^2 + 4E_1^2) \right] \quad (\text{B14})$$

$$\mathcal{E} = p_0^2 \left[ (p_0^2 + 4E_1^2) (u + m_1^2 - m_2^2) + 4E_1^2 (p_0^2 - k_0^2 + u) \right] \quad (\text{B15})$$

$$\begin{aligned} \mathcal{F} &= (k_0^2 - m_1^2 + m_2^2)^2 (u - m_1^2 + m_2^2) + 4k_0^2 E_2^2 (u - m_1^2 + m_2^2) \\ &\quad - 4E_2^2 (k_0^2 - m_1^2 + m_2^2) (p_0^2 - k_0^2 - u) \end{aligned} \quad (\text{B16})$$

$$\mathcal{G} = 2E_1^2 (p_0^2 + k_0^2 - u) + p_0^2 (k_0^2 + m_1^2 - m_2^2) \quad (\text{B17})$$

and

$$\eta = k_0^2 + m_1^2 - m_2^2 \quad . \quad (\text{B18})$$

These expressions simplify somewhat in the case  $m_1 = m_2$ .

## REFERENCES

- [1] V. Bernard, N. Kaiser and U.-G. Meißner, Nucl. Phys. **B357**, 129 (1991).
- [2] V. Bernard, N. Kaiser and U.-G. Meißner, Nucl. Phys. **B364**, 283 (1991).
- [3] V. Bernard, N. Kaiser and U.-G. Meißner, Phys. Rev. **D43**, R2757 (1991).
- [4] M.K. Volkov and A.A. Osipov, Yad. Fiz. **34**, 1559 (1981), Preprint JINR-P2-83-490-mc.
- [5] M.J. Matison *et al.*, Phys. Rev. **D9**, 1872 (1974).
- [6] N.O. Johannesson and J.L. Petersen, Nucl. Phys. **B68**, 397 (1973).
- [7] A. Karabouraris and G. Shaw, J. Phys. **G6**, 583 (1980).
- [8] For reviews, see U. Vogl and W. Weise, Prog. Part. Nucl. Phys. **27**, 195 (1991); S.P. Klevansky, Rev. Mod. Phys. **64**, 649 (1992).
- [9] T. Hatsuda and T. Kunihiro, Phys. Rep. **247**, 241 (1994).
- [10] E. Quack and S.P. Klevansky, Phys. Rev. **C 49**, 3283 (1994).
- [11] V. Dmitrašinović, H.J. Schulze, R. Tegen and R.H. Lemmer, Ann. Phys. (N.Y.) **238**, 332 (1995).
- [12] E. Laermann, Nucl. Phys. **A610**, 1c (1996).
- [13] E. Laermann, Nucl. Phys. **B** (Proc. Suppl.) **60A** (1998) 180.
- [14] J. Müller and S.P. Klevansky, Phys. Rev. **C50**, 410 (1994).
- [15] S.P. Klevansky and R.H. Lemmer, Heidelberg Preprint HD-TVP-97/05.
- [16] H.-J. Hippe and S.P. Klevansky, Phys. Rev. **C52** (1995) 2172.

- [17] B. Bernard, U.-G. Meissner, A.H. Blin and B. Hiller, Phys. Lett. **B253** (1991) 443.
- [18] H.-J. Schulze, J. Phys. **G21** (1995) 185.
- [19] V. Bernard and D. Vautherin, Phys. Rev. **D40**, 1615 (1989).
- [20] P. Rehberg, S.P. Klevansky and J. Hüfner, Phys. Rev. **C53**, 410 (1996).
- [21] E. Quack, P. Zhuang, Y. Kalinovsky, S.P. Klevansky and J. Hüfner, Phys. Lett. **B348**, 1 (1995).
- [22] R.M Barnett et al., Phys. Rev. **D54**, 1 (1996).
- [23] J.L. Petersen, Phys. Rep. **2**, 155 (1971).
- [24] N. Nakanishi, *Graph Theory and Feynman Integrals* (Gordon and Breach, 1971).

TABLES

TABLE I. Parameter sets. The parameter sets denoted I and II correspond to those from Ref. [19] and which are similarly denoted therein. PR and HK designate the O(3) parameter sets used in Ref. [20] and Ref. [9] respectively.

|    | Renormalization | $m_{0q}$ (MeV) | $m_{0s}$ (MeV) | $\Lambda$ (MeV) | $G\Lambda^2$ | $K\Lambda^5$ |
|----|-----------------|----------------|----------------|-----------------|--------------|--------------|
| I  | Pauli-Villars   | 6.2            | 175            | 795             | 2.350        | 27.83        |
| II | Pauli-Villars   | 7.8            | 175            | 700             | 2.739        | 43.28        |
| PR | $O(3)$          | 5.5            | 140.7          | 602.3           | 1.835        | 12.36        |
| HK | $O(3)$          | 5.5            | 135.7          | 631.4           | 1.833        | 9.288        |

TABLE II. Quark and pseudoscalar meson masses at  $T = 0$ . The parameter set labels I, II, PR and HK are as described in Table I. Experimental values are given in the final row.

|     | $m_q$ (MeV) | $m_s$ (MeV) | $m_\pi$ (MeV) | $m_K$ (MeV) | $m_\eta$ (MeV) | $m_{\eta'}$ (MeV) |
|-----|-------------|-------------|---------------|-------------|----------------|-------------------|
| I   | 253.0       | 489.7       | 140.8         | 521.9       | 467.6          | 845.7             |
| II  | 367.8       | 557.4       | 140.0         | 485.9       | 497.3          | 1013.4            |
| PR  | 367.7       | 549.5       | 135.0         | 497.6       | 514.8          | 957.7             |
| HK  | 334.7       | 527.4       | 138.0         | 495.7       | 486.7          | 857.4             |
| Exp | -           | -           | 138           | 495         | 548            | 958               |



TABLE III. Scalar meson masses at  $T = 0$ . The parameter set labels I, II, PR and HK are as described in Table I. A tentative assignment of these masses to experimentally measured particles is given in the final row.

|     | $m_{\sigma_\pi}$ (MeV) | $m_{\sigma_K}$ (MeV) | $m_\sigma$ (MeV) | $m_{\sigma'}$ (MeV) |
|-----|------------------------|----------------------|------------------|---------------------|
| I   | 688.8                  | 904.6                | 510.7            | 1112.2              |
| II  | 890.8                  | 1073.4               | 735.4            | 1226.3              |
| PR  | 880.2                  | 1050.5               | 728.9            | 1198.3              |
| HK  | 792.4                  | 980.0                | 667.8            | 1149.9              |
| Exp | $a_0(980)$             | $K_0^*(1430)$        | $f_0(980)$       | $f_0(1300)$         |

TABLE IV. Contributions to the scattering length  $a_0^{3/2}$  in units of  $m_\pi$  at  $T = 0$ . The parameter set labels I, II, PR and HK are as described in Table I.

| Parameter Set | box     | $t$ channel | $u$ channel | sum     |
|---------------|---------|-------------|-------------|---------|
| I             | -0.3689 | 0.2224      | 0.1091      | -0.0375 |
| II            | -0.6454 | 0.4577      | 0.1587      | -0.0289 |
| PR            | -0.7047 | 0.5332      | 0.1741      | -0.0025 |
| HK            | -0.6000 | 0.4000      | 0.1771      | -0.0230 |

TABLE V. Contributions to the scattering length  $a_0^{1/2}$  in units of  $m_\pi$  at  $T = 0$ . The parameter set labels I, II, PR and HK are as described in Table I.

| Parameter Set | box     | $t$ channel | $u$ channel | sum    |
|---------------|---------|-------------|-------------|--------|
| I             | -0.2255 | 0.2224      | 0.1296      | 0.1265 |
| II            | -0.4706 | 0.4577      | 0.1447      | 0.1318 |
| PR            | -0.5108 | 0.5332      | 0.1572      | 0.1795 |
| HK            | -0.4195 | 0.4000      | 0.1710      | 0.1515 |

## FIGURES

FIG. 1. Six possible box diagrams that contribute to meson-meson scattering. Double lines denote mesons, while the internal single lines depict the quark structure.

FIG. 2. Three possible meson exchange graphs, corresponding to  $s$ ,  $t$  and  $u$  channels respectively. The double lines represent mesons and the single lines represent quarks.

FIG. 3. The only box diagram contributing to the elastic scattering amplitude  $\pi^+K^+ \rightarrow \pi^+K^+$ . Here we denote the mesonic states with double lines and quarks by single lines. The  $s$  quark is denoted by a heavy single quark.

FIG. 4. Possible  $t$  channel meson exchange diagrams that contribute to the scattering  $\pi^+K^+ \rightarrow \pi^+K^+$ . Mesonic states are denoted by double lines, quarks by single lines. The  $s$  quark is denoted by a heavy single line.

FIG. 5. Generic three meson vertex function  $\Gamma_1^{12}$  that occurs in the  $t$  channel. The external double lines denote meson states. The internal single lines denote quarks with masses  $m_1$  or  $m_2$  as indicated.

FIG. 6.  $u$  channel graph for the scattering amplitude  $\pi^+K^+ \rightarrow \pi^+k^+$ . External double lines represent mesons, while single lines represent quarks. The  $s$  quark is represented by a heavy single line.

FIG. 7. Generic three meson vertex function  $\Gamma_2^{12}$  that occurs in the  $u$  channel. External double lines represent mesons, while single lines denote quarks with masses  $m_1$  or  $m_2$  as indicated.

FIG. 8. Pseudoscalar meson masses versus temperature for the parameter set labeled HK of Table I. Shown are  $m_\pi$  (solid line),  $m_K$  (dashed line), and  $m_\eta$  (lower dot-dashed line). The combinations  $m_\pi + m_K$  (dotted line) and  $m_q + m_s$  (upper dot-dashed line) are also shown.  $T_{\pi K}$  and  $T_{MK}$  are indicated with arrows.

FIG. 9. Scalar meson masses versus temperature for the parameter set labeled HK. Shown are  $m_\sigma$  (dotted line),  $m_{\sigma_\pi}$  (solid line),  $m_{\sigma_K}$  (dashed line) and  $m_{\sigma'}$  (dot-dashed line).

FIG. 10. Temperature dependence of  $a_0^{3/2}$  as well as the decomposition of the  $t$ ,  $u$  and box graph contributions to this quantity for the parameter set of HK, in units of  $m_\pi$ . The full curve for  $a_0^{3/2}$  is indicated by the solid line, the box diagram contribution by dashed lines, the  $t$  and  $u$  contributions by a dotted and dot-dashed curve respectively.

FIG. 11. Temperature dependence of  $a_0^{1/2}$  as well as the  $t$ ,  $u$  and box graph contributions to this quantity for the parameter set of HK and in units of  $m_\pi$ . The full curve for  $a_0^{1/2}$  is indicated by the solid line, the box diagram contribution by dashed lines, the  $t$  and  $u$  contributions by a dotted and dot-dashed curve respectively.

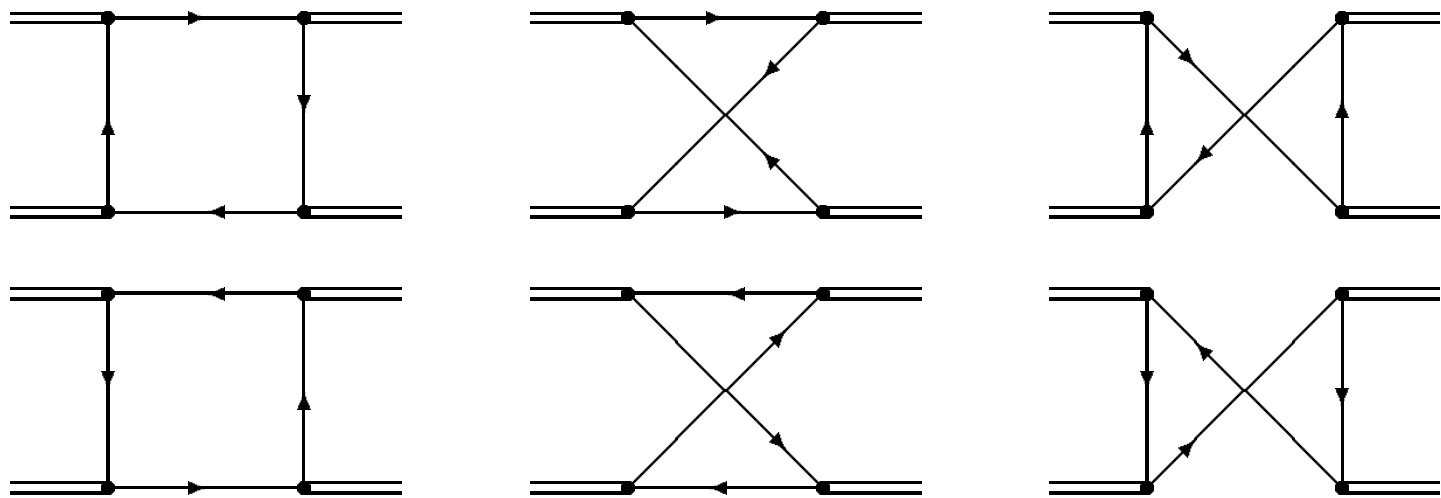


Figure 1

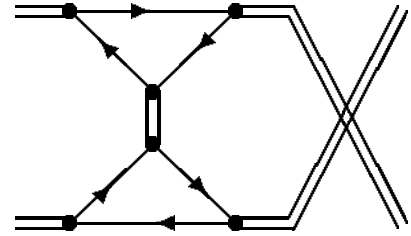
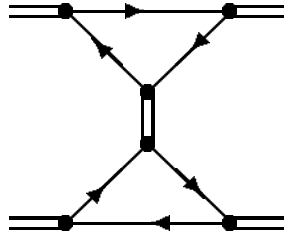
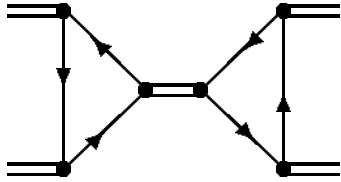


Figure 2

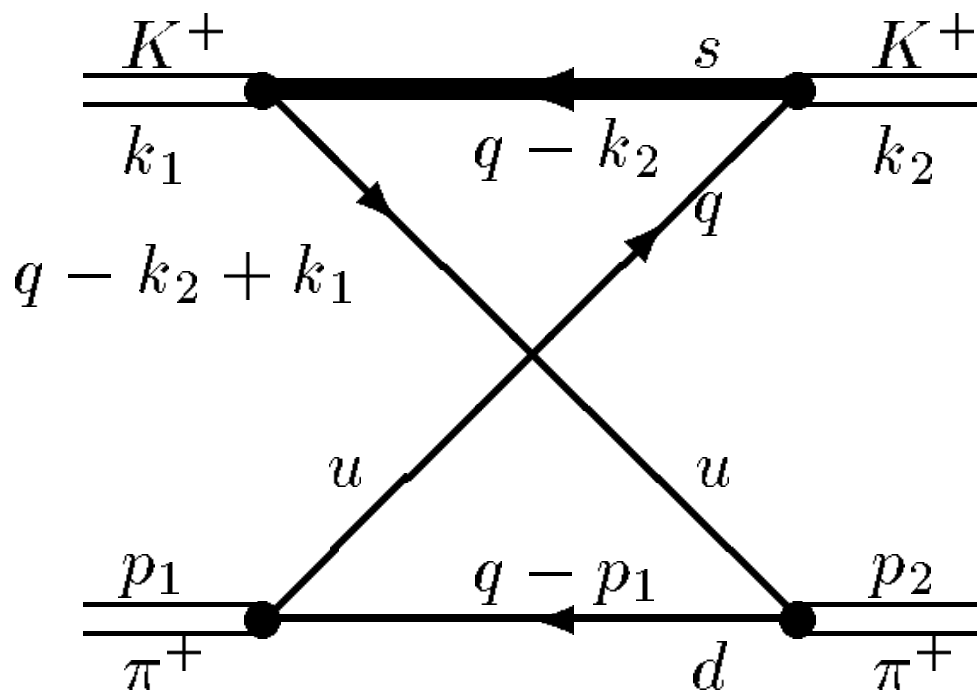


Figure 3

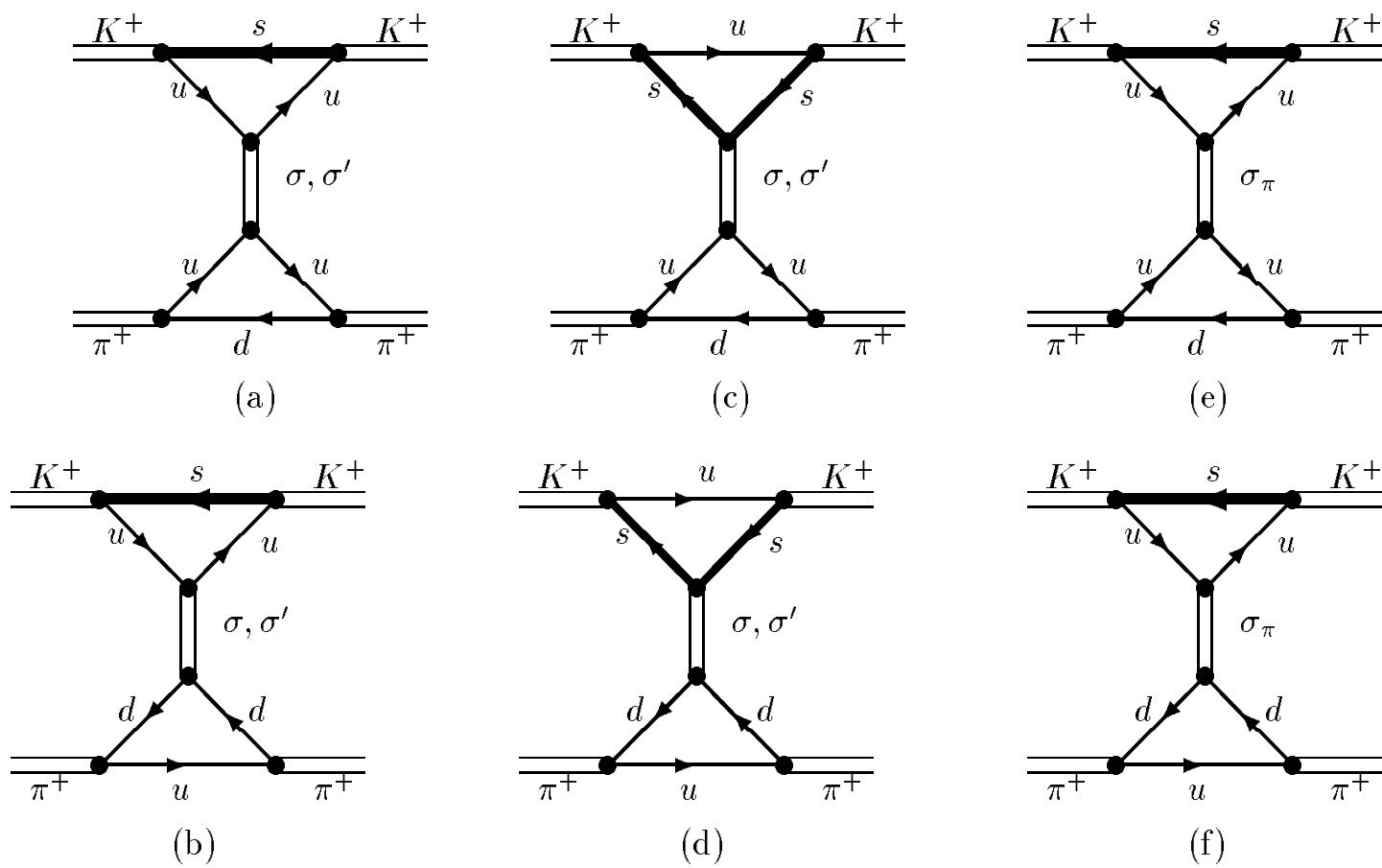


Figure 4

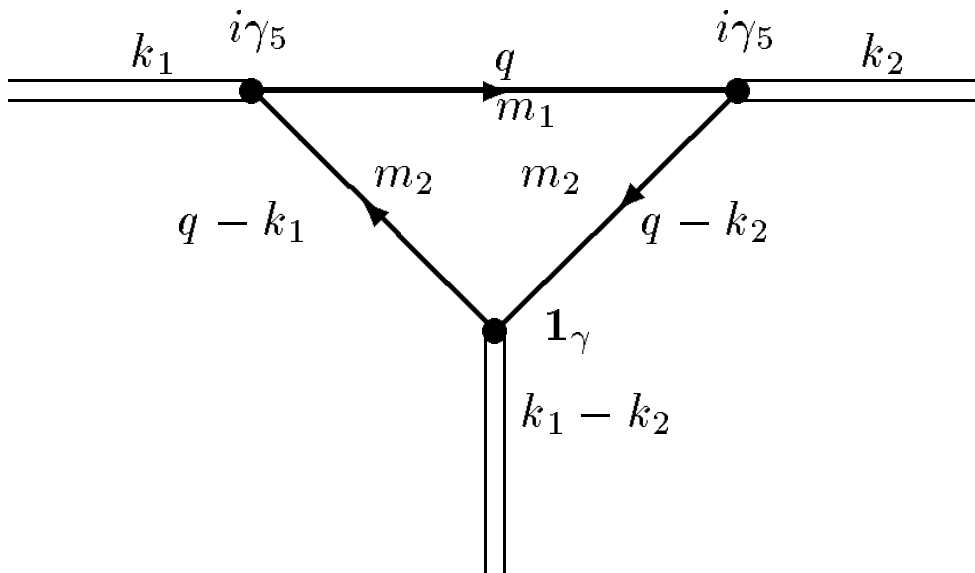


Figure 5



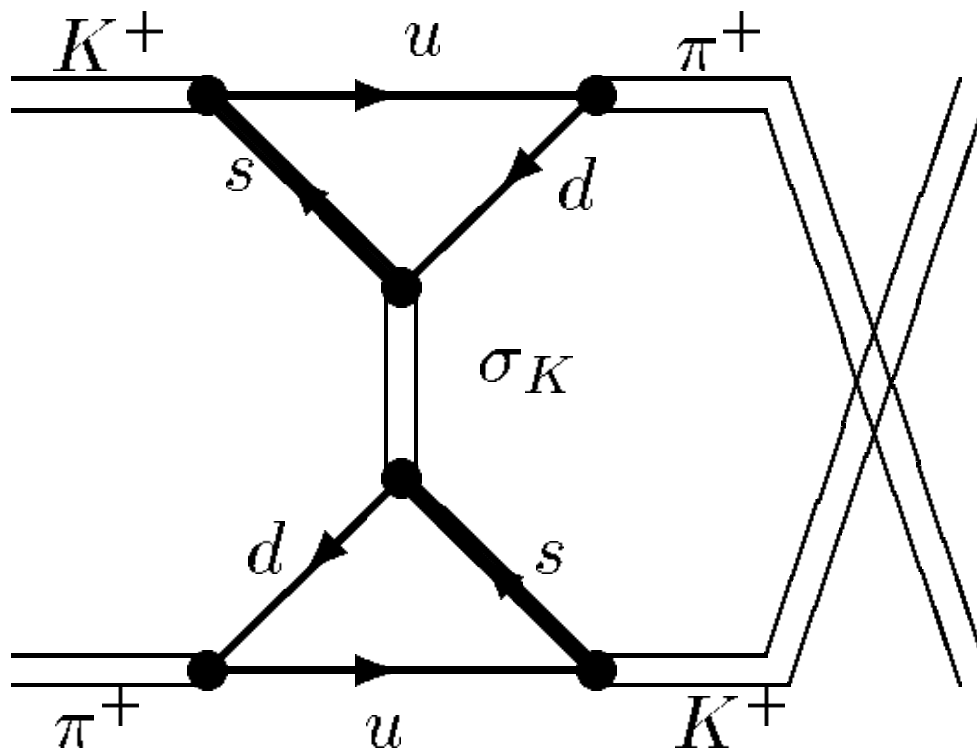


Figure 6

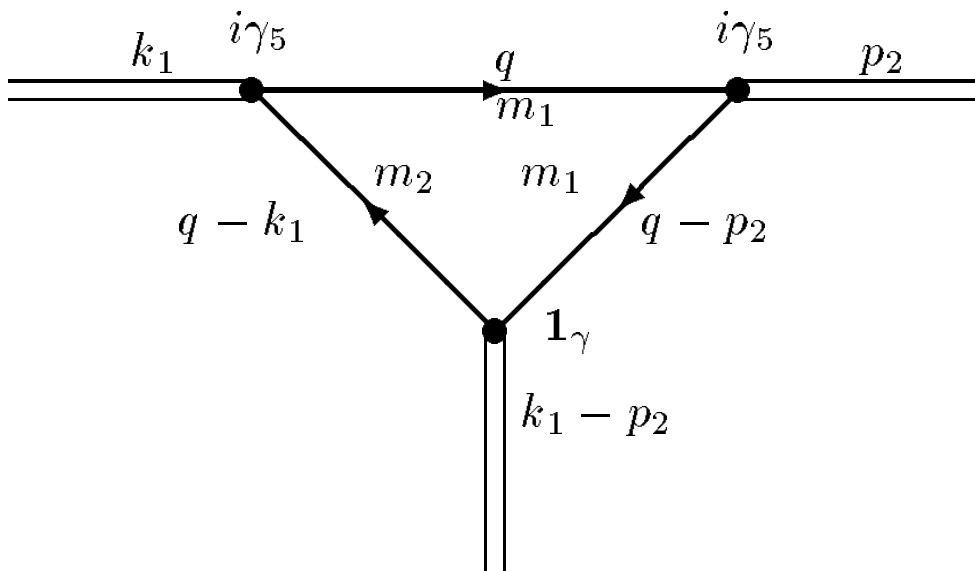


Figure 7

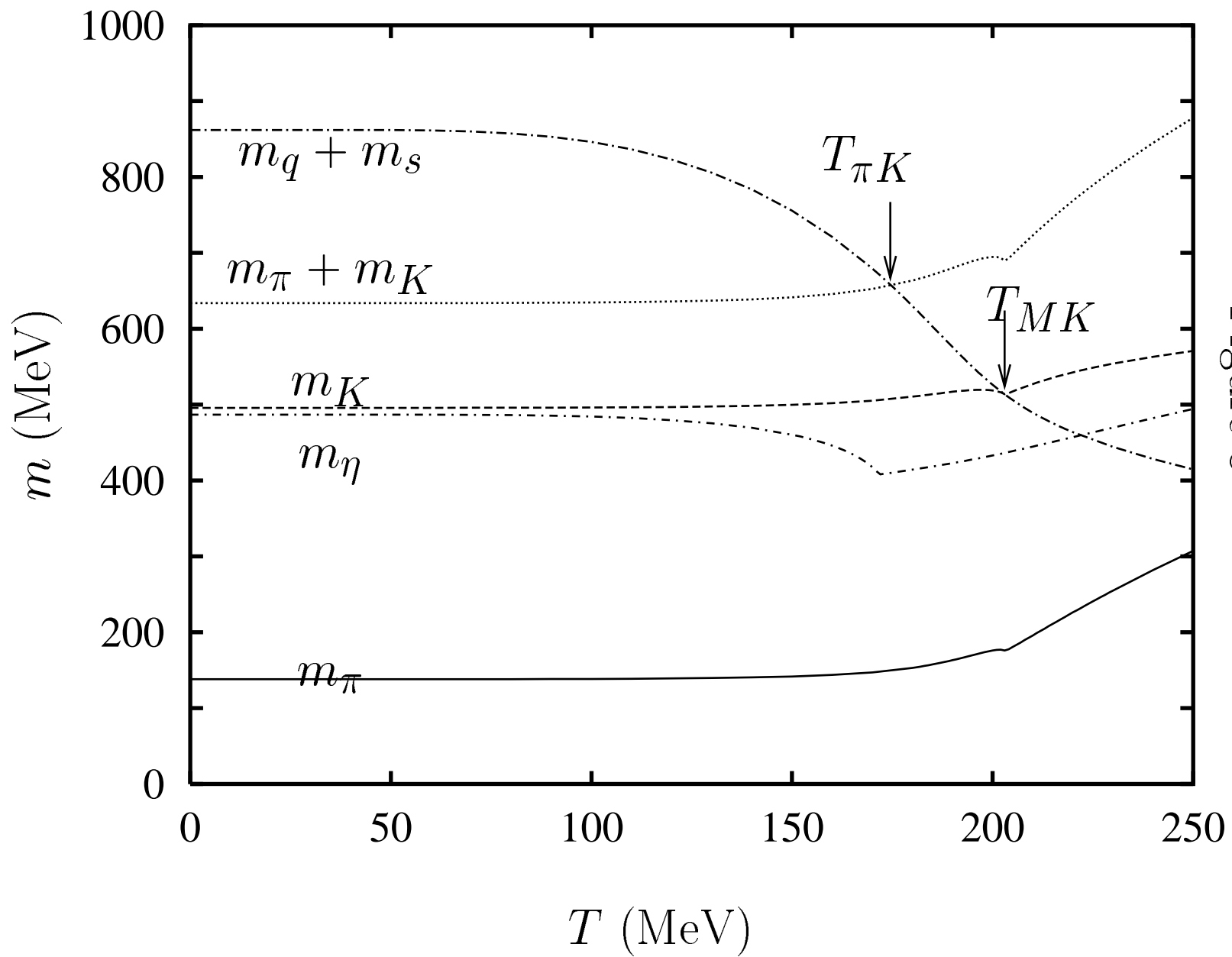


Figure 8

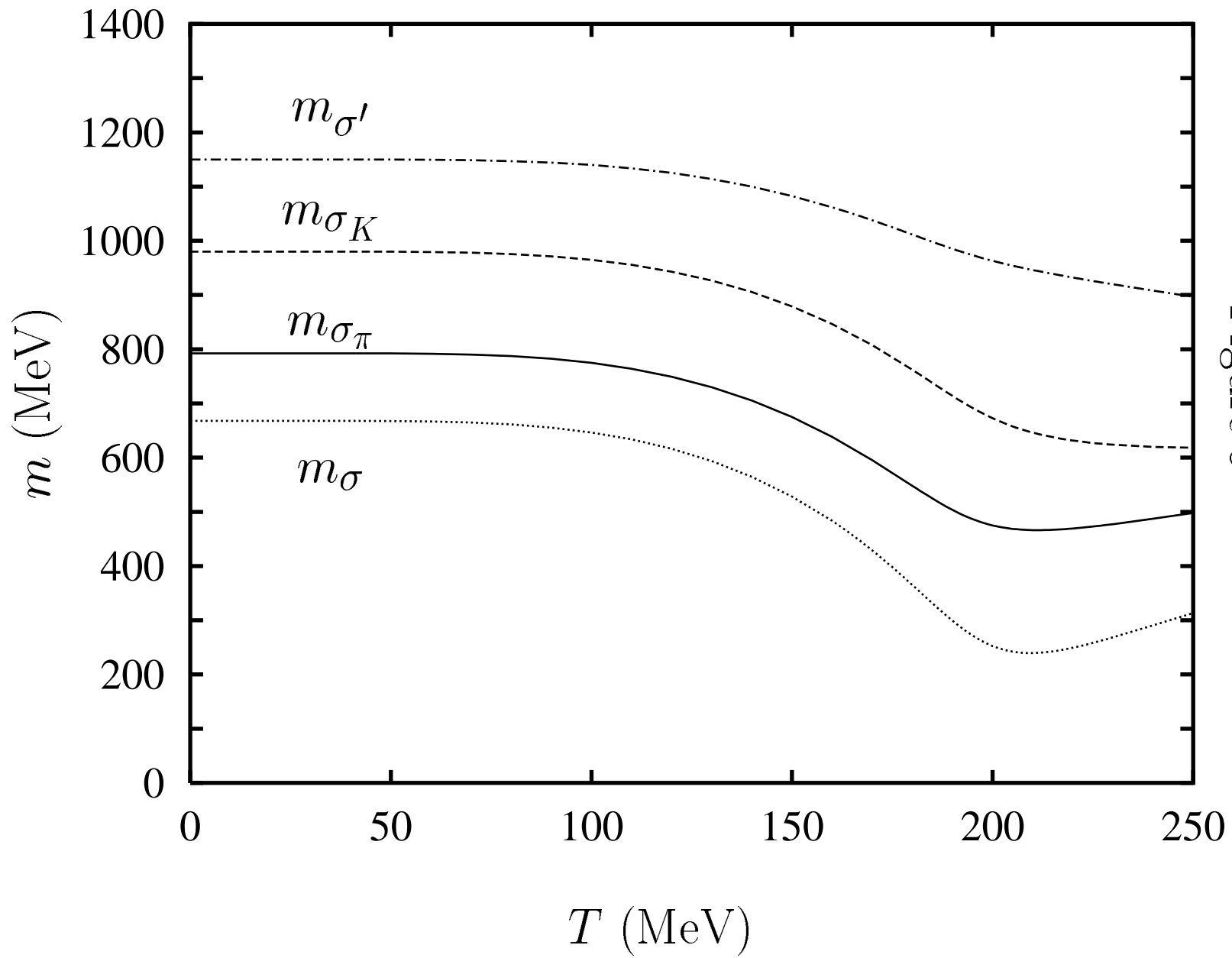


Figure 9

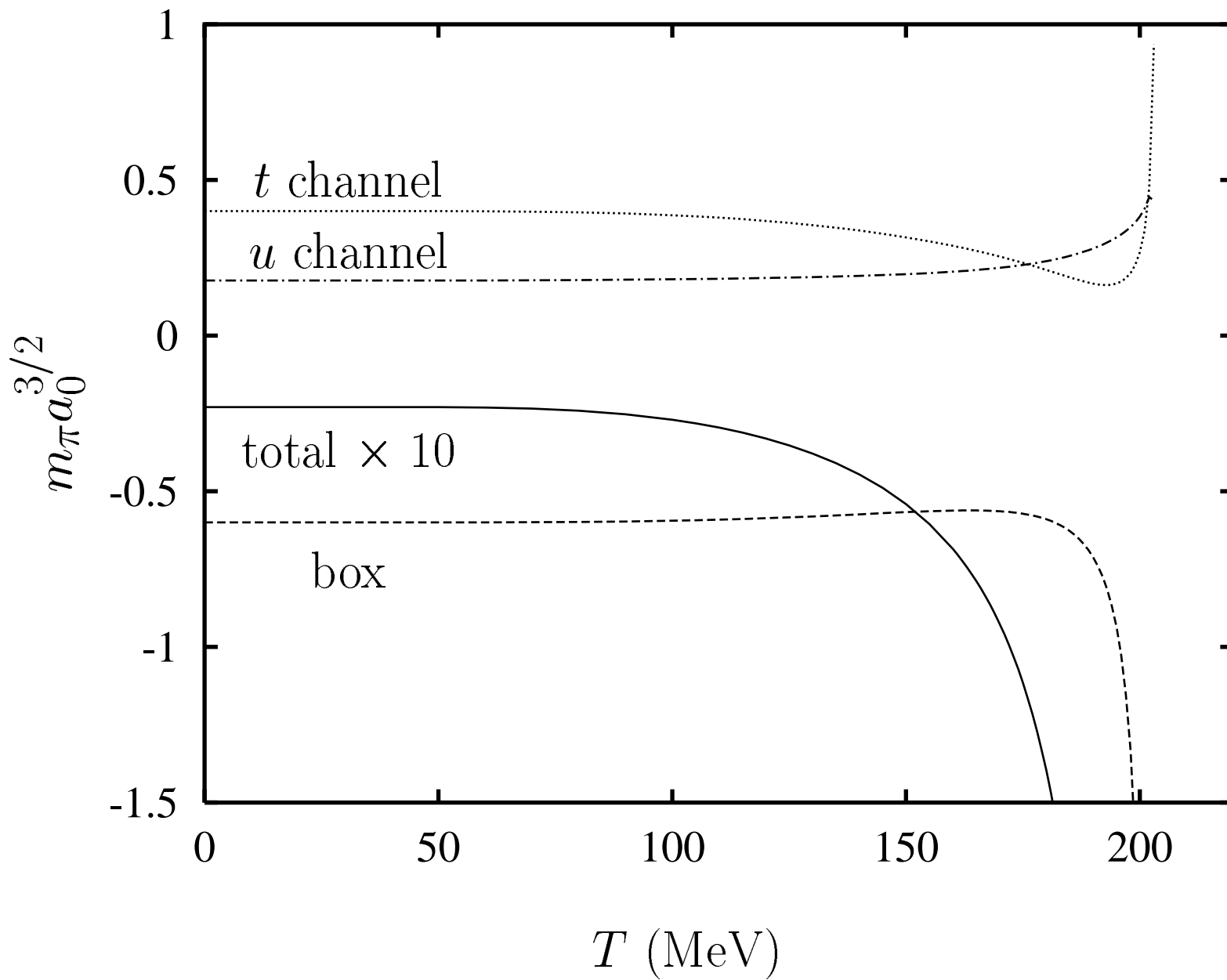


Figure 10

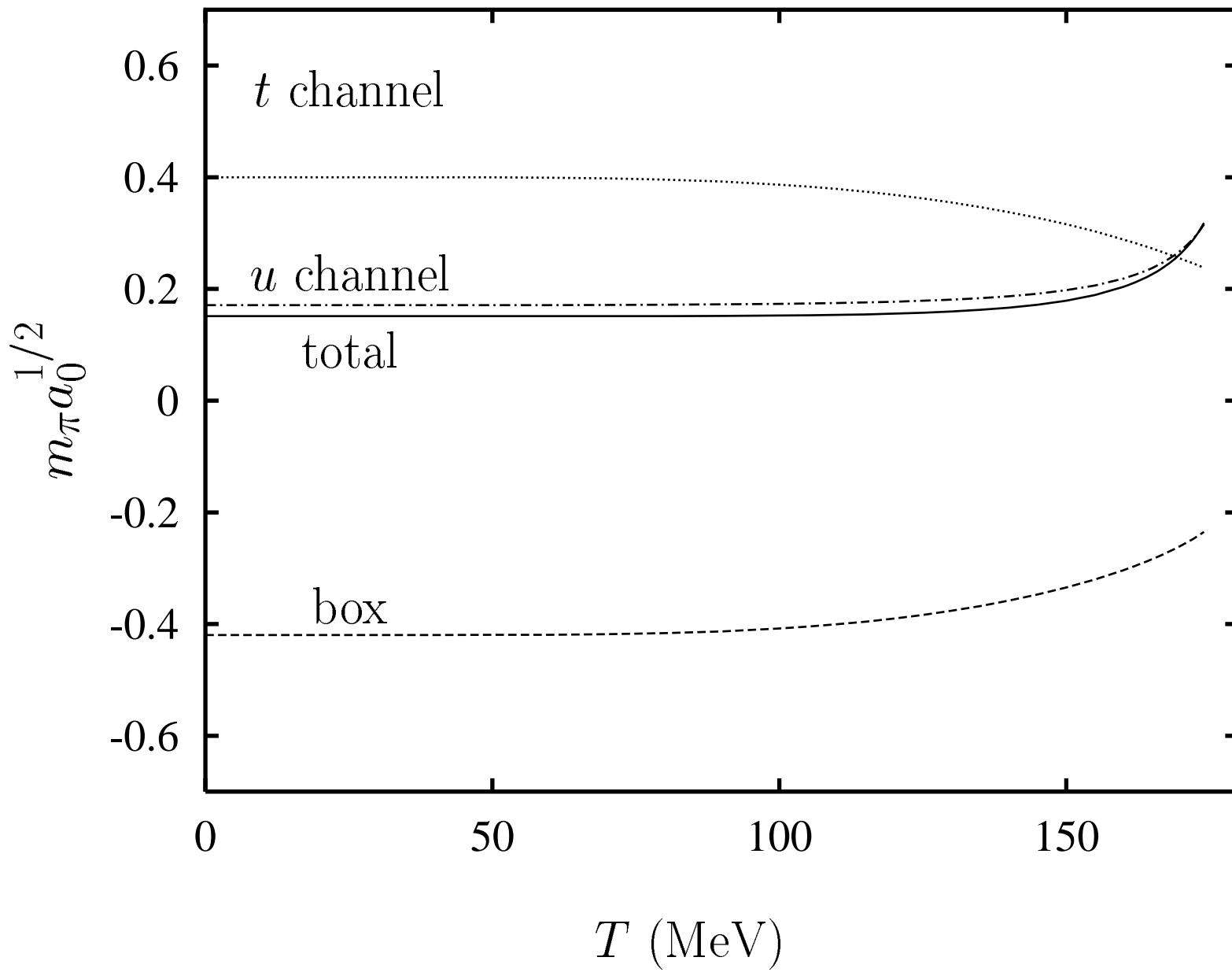


Figure 11